

# Reversible addition of the OH radical to *p*-cymene in the gas phase: kinetic analysis assuming formation of a single adduct. Part 1

Cite this: *Phys. Chem. Chem. Phys.*, 2013, **15**, 20105

Paulo Alarcón,<sup>a</sup> Rafal Strekowski<sup>b</sup> and Cornelius Zetzsch<sup>\*ac</sup>

A flash photolysis-resonance fluorescence (FP-RF) technique was employed to study the kinetics and mechanism of the reaction of OH radicals with *p*-cymene at temperatures between 297 and 413 K in helium buffer gas. FP-RF experiments involved time-resolved detection of OH radicals by RF following vacuum-UV flash photolysis of H<sub>2</sub>O–*p*-cymene–He and H<sub>2</sub>O–He mixtures. Biexponential functions were fitted to decays of OH radicals according to reversible addition of OH radicals to *p*-cymene to form a single adduct. A rate constant of  $(15.7 \pm 1.1) \times 10^{-12}$  is obtained (in units of cm<sup>3</sup> s<sup>-1</sup>) at room temperature (298 K) for the sum of the addition and abstraction channels ( $k_{1a} + k_{1b}$ ) according to this simplified model. The Arrhenius plot reveals the step function typical of other aromatics and can be described using the expressions:  $2 \times 10^{-13} \exp(+1300 \text{ K}/T)$  at temperatures between 297 K and 324 K and  $10^{-11} \exp(-250 \text{ K}/T)$  at temperatures between 345 K and 413 K. After consideration of the abstraction channel an equilibrium constant of  $k_{1a}/k_{-1a} = 6 \times 10^{-26} \exp(+9700 \text{ K}/T) \text{ cm}^3$  is obtained at temperatures between 297 and 325 K and  $2 \times 10^{-36} \exp(+17000 \text{ K}/T) \text{ cm}^3$  at temperatures between 325 and 380 K.

Received 19th July 2013,

Accepted 20th September 2013

DOI: 10.1039/c3cp53040j

[www.rsc.org/pccp](http://www.rsc.org/pccp)

## 1. Introduction

Total regional and global emissions of biogenic compounds have been estimated to be equivalent to or exceed anthropogenic non-methane hydrocarbon emissions.<sup>1,2</sup> Once emitted into the atmosphere, these biogenic compounds react readily with atmospheric OH radicals to play an important role in tropospheric chemistry including the boundary layer ozone formation in urban and rural settings. However, to date the observed high ozone creation potential of biogenic compounds and even more so of aromatics remains poorly characterized and not fully understood.

The aromatic molecule *p*-cymene (1-methyl-4-isopropyl-benzene) is a compound of biogenic origin emitted into the atmosphere from vegetation. It has been established that direct emissions from vegetation are a major atmospheric source of *p*-cymene.<sup>3–5</sup> Field observations of *p*-cymene emissions from a northern coniferous forest in the United States estimate fluxes of up to  $28 \mu\text{g C m}^{-2} \text{ h}^{-1}$ , representing about 3% of the total emissions in the northern coniferous forest.<sup>6</sup>

Indirect emissions of *p*-cymene can also occur from the atmospheric transformation of  $\alpha$ -pinene.<sup>7</sup> Laboratory experiments

of *p*-cymene formation in a teflon chamber gave yields of up to 0.12% at 70% relative humidity using acid conditioned walls. Transposing this finding *via* the surface/volume ratio of the chamber to environmental conditions, these authors suggested a contribution to the *p*-cymene emission flux in the northern coniferous forest of up to  $0.23 \mu\text{g C m}^{-2} \text{ h}^{-1}$ . Furthermore, Aschmann *et al.*<sup>8</sup> determined the formation of *p*-cymene from the oxidation of the structurally related  $\gamma$ -terpinene by OH radicals with a molar yield of  $13.6 \pm 2.5\%$ , suggesting a contribution to the *p*-cymene flux up to  $0.11 \mu\text{g C m}^{-2} \text{ h}^{-1}$  in the northern coniferous forest, where the direct emissions were estimated to constitute up to  $0.8 \mu\text{g C m}^{-2} \text{ h}^{-1}$ .<sup>6</sup>

The atmospheric fate of *p*-cymene is governed by OH radical addition to the aromatic ring and H-atom abstraction from the isopropyl and methyl groups. *p*-Cymene is not expected to be significantly degraded by oxygen atoms ( $\text{O}^3\text{P}$ ), ozone ( $\text{O}_3$ ) or  $\text{NO}_3$  because of its plain aromatic structure. The calculated tropospheric lifetimes of *p*-cymene toward the atmospheric attack by ozone during the day and  $\text{NO}_3$  at night are >330 days and 1.3 years, respectively.<sup>9</sup> Its reaction with OH radicals is believed to be the most important atmospheric removal process of *p*-cymene. In addition to the interest in the fundamental properties of the OH + *p*-cymene reaction, an understanding of the relevant *p*-cymene sinks would enhance our knowledge of the atmospheric chemistry of *p*-cymene, that is, ozone and secondary organic aerosol (SOA) formation potentials.

To date, only one laboratory kinetic study reports the room temperature rate constant for the reaction of OH radicals

<sup>a</sup> Atmospheric Chemistry Research Laboratory, University of Bayreuth, 95448, Bayreuth, Germany. E-mail: [cornelius.zetzsch@uni-bayreuth.de](mailto:cornelius.zetzsch@uni-bayreuth.de)

<sup>b</sup> Aix-Marseille Univ. Laboratoire Chimie Environnement, FRE 3416, Marseille, France

<sup>c</sup> Fraunhofer-Institute for Toxicology and Experimental Medicine, 30625 Hannover, Germany

with *p*-cymene. Corchnoy and Atkinson<sup>9</sup> used a relative rate method and report  $k = 1.51 \times 10^{-11} \text{ cm}^3 \text{ s}^{-1}$  at 295 K for the OH + *p*-cymene reaction, using cyclohexane as the reference reaction ( $k_{\text{cyclohexane}+\text{OH}} = 7.43 \times 10^{-12} \text{ cm}^3 \text{ s}^{-1}$ ) that results in a tropospheric lifetime of *p*-cymene toward the attack by OH radicals of about 1 day. Recently, the mechanism of the OH + *p*-cymene reaction has been studied at room temperature by Aschmann *et al.*<sup>10</sup> These investigators report that the H-atom abstraction from the isopropyl group accounts for  $14.8 \pm 3.2\%$  and that the sum of abstraction from the methyl and isopropyl groups accounts for  $20 \pm 4\%$  of the total rate constant for the OH + *p*-cymene reaction at 298 K. In this work, we use a direct, *in situ* and real-time flash photolysis-resonance fluorescence (FP-RF) technique to study the OH + *p*-cymene reaction as a function of temperature over the range 297–413 K in helium buffer gas.

## 2. Experimental

The experimental methodology, originally developed by Stuhl and Niki<sup>11</sup> and since then employed by various other authors,<sup>12–17</sup> couples radical production by vacuum-UV flash photolysis (FP) with sensitive time-resolved detection of OH using resonance fluorescence (RF). The experimental approach is similar to a number of other studies on OH radical reactions of atmospheric interest.<sup>18–30</sup> The experiments involved time-resolved detection of OH radicals by resonance fluorescence ( $A^2\Sigma^+ \rightarrow X^2\Pi$ ) at  $\lambda = 308 \text{ nm}$  following vacuum-UV flash photolysis of H<sub>2</sub>O–*p*-cymene–He and H<sub>2</sub>O–He mixtures. The schematic diagram of the FP-RF apparatus is shown in Fig. 1. Details of the experimental approach are given below.

A black anodized aluminium reaction cell was used in all experiments which were carried out under precisely known temperature, pressure and flow conditions. The reaction cell has been described in detail by Witte *et al.*,<sup>21</sup> and was maintained at a constant temperature ( $\pm 1 \text{ K}$ ) by circulating silicone oil from a temperature controlled bath through the double-walled Wood's horns and the body of the cell. A platinum resistance thermometer, Pt-100, close to the reaction zone, allowed the measurement of the temperature of the experiments. The geometry of the reaction cell and the gas saturation system has been described in detail by Wahner and Zetzsch.<sup>18</sup> The vacuum UV (VUV) beam and the resonance lamp beam enter the cell perpendicular to one another and to the photomultiplier, *i.e.*, the RF detector is orthogonal to the overlapping beams. The direction of the gas flow was perpendicular to the direction of both the photolyzing VUV beam and the photomultiplier tube (PMT) detector.

A few initial experiments were performed using a home-made flash lamp with a spark discharge (at a distance of 25 cm from the observation zone) in N<sub>2</sub> with a flash energy of 600 mJ calculated using 0.01  $\mu\text{F}$  capacitance (Type EC 103 50 M Condenser Products) and 11 kV applied voltage. However, in the majority of the experiments a Perkin Elmer FX 1165 short arc xenon flash lamp with a MgF<sub>2</sub> window served as the photolytic light source to generate the OH radicals from the FP of H<sub>2</sub>O. Typical xenon flash lamp energies ranged from 60 to 540 mJ. The lamp spark gap was mounted at a distance of 7.5 cm from the observation zone,

and the VUV beam entered the reaction cell through another MgF<sub>2</sub> window, where the space between the MgF<sub>2</sub> windows (2.5 cm) was constantly flushed by N<sub>2</sub> gas from the liquid nitrogen reservoir of the laboratory. A quartz resonance lamp mounted at right angles to the VUV photolysis beam excited the photolytically produced OH radicals in the reaction cell volume by resonance fluorescence. Optimized optical systems of two plano convex lenses each, (diameter = 38 mm, antireflection-coated for 308 nm), were used for imaging the plasma of the resonance lamp into the center of the fluorescence cell and for collecting the resulting resonance fluorescence onto the photocathode of the photomultiplier. An additional Al coated spherical mirror 5 cm in radius was mounted at the rear of the RF lamp and served to enhance the lamp emission intensity. The microwave power was supplied by a microwave generator (Muegge, Reichelsheim, MW-GPRYJ1511-300-01, 2.45 GHz, 300 W) *via* a water cooled circulator (Philips, Type 2722 163 02071) and operated at  $\sim 70 \text{ W}$ . A gas mixture of H<sub>2</sub>O–He at a total pressure of 130 mbar was allowed to flow through the resonance lamp. The electrodeless microwave discharge dissociated H<sub>2</sub>O to produce OH radicals. These radicals were then electronically excited to the  $A^2\Sigma^+$  state *via* collisions with either electronically excited He or free electrons. Since the fluorescence is resonant, the  $A^2\Sigma^+ \rightarrow X^2\Pi$  radiation leaving the lamp electronically excites OH ( $X^2\Pi$ ) radicals present in the reaction vessel. The resulting resonance fluorescence ( $A^2\Sigma^+ \rightarrow X^2\Pi$ ) at 308 nm was coupled out of the lamp through two quartz lenses (Heraeus, Suprasil,  $f_{\text{VIS}} = 50 \text{ mm}$ ) into the reaction cell. The resonance fluorescence light was collected by another anti-reflection coated quartz lens (Heraeus, Suprasil,  $f_{\text{VIS}} = 50 \text{ mm}$ ) and passed through a 308 nm interference filter (FWHM = 9 nm) which blocked impurity emissions from the resonance lamp radiation on the axis normal to both the photolysis VUV beam and the resonance lamp beam and was imaged by another quartz lens (Heraeus, Suprasil,  $f_{\text{VIS}} = 50 \text{ mm}$ ) onto the photocathode of a photomultiplier tube (Thorn-EMI, 9789QB). The signal was processed and accumulated using photon-counting techniques in conjunction with multichannel scaling (EG&G Ortec, model ACE MCS) and saved in a PC.

All experiments were carried out under “slow flow” conditions with a mean linear flow rate of about  $1 \text{ cm s}^{-1}$  at 200 mbar and a VUV flash repetition rate of 0.2 Hz, so that the gas mixture within the detection volume was replenished between VUV flashes. The gases used in this work had the following stated minimum purities: He (Riessner) – 99.996%; liquid N<sub>2</sub> (Linde) – 99.999%. The liquid *p*-cymene (Aldrich) had a stated minimum purity of 99%. Deionized water was doubly distilled by a quartz still. Concentrations of H<sub>2</sub>O and *p*-cymene in the reaction mixture were calculated from the given vapour pressures, temperature, mass-flow rates and total pressure. The Antoine equation for the vapour pressure of H<sub>2</sub>O used in this study was  $\log_{10}[P(\text{mbar})] = 5.40221 - [1838.675/(T(\text{K}) - 31.737)]$ .<sup>31</sup> For *p*-cymene the saturator was kept at  $T = 293 \text{ K}$ . Literature data of the vapour pressure are available for temperatures between 268 and 286 K,<sup>32</sup> between 300 and 450 K,<sup>33</sup> between 381 and 452 K,<sup>34</sup> and between 314 and 452 K,<sup>35</sup> but no direct measurements have been reported near room temperature. Ruzicka Jr. *et al.*<sup>36</sup> reviewed vapour pressure

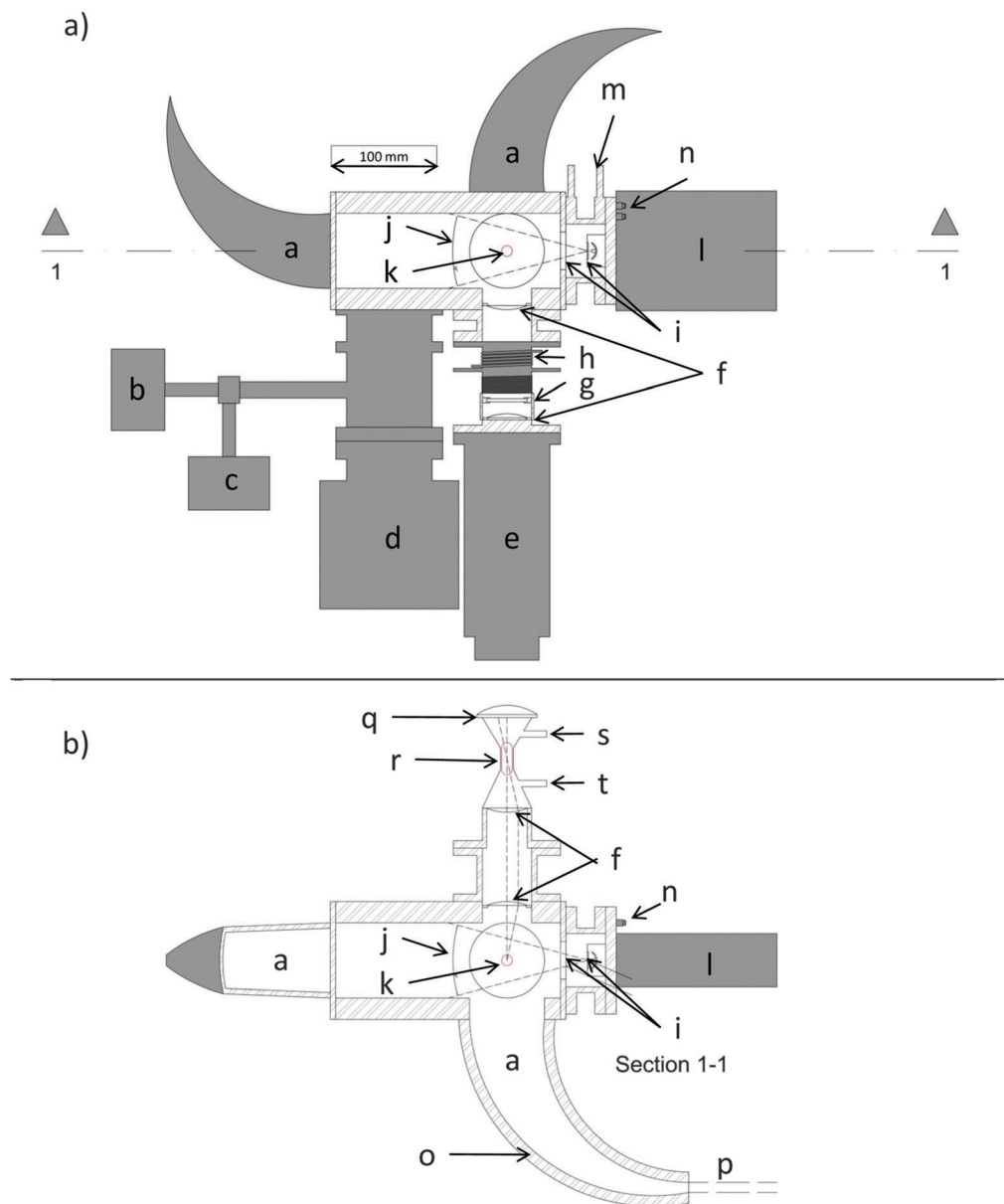


**Fig. 1** Top (a) and side (b) views of the flash photolysis resonance fluorescence (FR-RF) system used in this work. (a) Wood's horn; (b) pressure gauge (10 Torr); (c) pressure gauge (1000 Torr); (d) vacuum valve; (e) photomultiplier; (f) focusing lenses; (g) interference filter (308 nm); (h) focusing screw; (i) MgF<sub>2</sub> windows; (j) 60% intensity compared to the central beam; (k) observation zone; (l) lamp power supply; (m) N<sub>2</sub> purge gas inlet; (n) lamp water cooling; (o) mantle with silicon oil circulating from a thermostat; (p) gas mixture inlet; (q) concave mirror; (r) microwave discharge; (s) resonance lamp He–H<sub>2</sub>O mixture outlet and (t) inlet.

data for *p*-cymene and a group of other high-boiling alkylbenzenes at temperatures between 223.15 and 323.15 K determined by direct measurements at pressures higher than 1 kPa and related thermodynamic data, where the recommended pressure for *p*-cymene has been calculated using the Cox eqn (1)

$$\ln\left(\frac{P_{\text{sat}}}{P_0}\right) = \left(1 - \frac{T_0}{T}\right) \exp(A_0 + A_1 T + A_2 T^2) \quad (1)$$

with the following parameters:  $A_0 = 2.82209$ ;  $A_1 = -1.438828 \times 10^{-3}$ ;  $A_2 = 1.191725 \times 10^{-6}$ ; with  $T_0 = 450.259$  K and  $P_0 = 101.325$  kPa. The calculated *p*-cymene vapour pressure was found to be in good agreement with direct measurements below 268 K<sup>32</sup> and

above 300 K<sup>33</sup> within a 10% deviation, leading to a vapour pressure of  $1.44 \pm 0.14$  mbar at 293 K.

The initial OH radical concentration produced by VUV photolysis of H<sub>2</sub>O at  $1.5 \times 10^{15}$  cm<sup>-3</sup> using the N<sub>2</sub> spark discharge lamp was estimated by Koch *et al.*,<sup>26</sup> comparing signal intensities corrected for fluorescence quenching by H<sub>2</sub>O with measurements of Witte *et al.*,<sup>21</sup> and leading to a concentration well below 10<sup>10</sup> cm<sup>-3</sup> at 2 J flash energy. A FP-RF with similar geometry<sup>18</sup> was used by Zhang *et al.* at the University of Aix-Marseille<sup>27,28,30</sup> to study other OH radical reactions of atmospheric interest. These investigators determined the initial OH concentration using a Xe flash lamp at

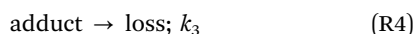
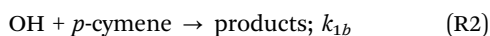
540 mJ flash energy and measured the ozone concentration after the photolysis of a 20% O<sub>2</sub>-N<sub>2</sub> mixture to estimate a maximum value for the initial OH concentration of  $2 \times 10^{10} \text{ cm}^{-3}$  under the experimental conditions employed. These and our OH radical concentrations are two orders of magnitude smaller than the smallest concentration of *p*-cymene used in this work, ensuring pseudo-first-order conditions.

The temperature within the reactor was varied between 297 K and 413 K, and the total pressure was varied between 185 and 596 mbar He.

### 3. Results and discussion

#### 3.1 Kinetic analysis and data evaluation

The behaviour of OH radicals in the presence of *p*-cymene in our system is described *via* a number of reaction channels, including reversible adduct formation, abstraction and other loss processes of OH and the adduct:



The rate equations that describe the change in the concentrations of OH radicals and the adduct (that regenerates OH) as a function of time are the following:

$$\frac{d}{dt}[\text{OH}] = -a[\text{OH}] + b[\text{add}] \quad (2)$$

$$\frac{d}{dt}[\text{add}] = c[\text{OH}] - d[\text{add}] \quad (3)$$

where the combined first-order rate constants are  $a = k_2 + (k_{1a} + k_{1b})[p\text{-cymene}]$ ,  $b = k_{-1a}$ ,  $c = k_{1a}[p\text{-cymene}]$ , and  $d = k_{-1a} + k_3$ . The analytical solution of the system of differential equations has been published by Wahner and Zetzsch,<sup>18</sup> and the expressions for obtaining  $a$ ,  $d$  and the product  $bc$  from the observed biexponential decays rates and intensity ratios<sup>29</sup> are given below in eqn (4)–(6).

$$bc = \frac{(\tau_1^{-1} - \tau_2^{-1})^2 \left(\frac{I_1}{I_2}\right)}{\left(1 + \frac{I_1}{I_2}\right)^2} \quad (4)$$

$$a = \frac{\tau_1^{-1} \left(\frac{I_1}{I_2}\right) + \tau_2^{-1}}{1 + \left(\frac{I_1}{I_2}\right)} \quad (5)$$

$$d = \frac{\tau_2^{-1} \left(\frac{I_1}{I_2}\right) + \tau_1^{-1}}{1 + \left(\frac{I_1}{I_2}\right)} \quad (6)$$

Fit parameters obtained for the decay curves of each experiment can be used in eqn (4)–(6) to determine the rate constants  $a$ ,

$bc$  and  $d$ . Linear fits of  $a$  and  $bc$ , for a given temperature, against the concentration of *p*-cymene allowed us to determine  $k_2$  and the sum  $k_{1a} + k_{1b}$  from  $a$  as the intercept  $a_0$  and the slope and the product  $k_{1a} k_{-1a}$  from  $bc$ . However, the evaluation of individual biexponential decays in the presence of a fixed concentration of *p*-cymene (so-called “*e*-fit”, see Koch *et al.*<sup>26</sup>) runs into problems if the intensity ratios become too large or too small and if  $\tau_1^{-1}$  and  $\tau_2^{-1}$  become similar in certain concentration ranges of *p*-cymene, due to the then large mutual covariances of the exponential parameters.

Koch *et al.*<sup>26</sup> improved the evaluation method by fitting sets of biexponential decays at various concentrations but at the same temperature simultaneously to the biexponential model (so-called “*k*-fits”). The fitting program used in this work follows the same concept and was developed using IDL (Interactive Data Language, Research Systems Inc.).<sup>29</sup> Similar to the procedure described by Bohn and Zetzsch,<sup>29</sup> errors were estimated by varying the combined first-order rate constants until the measured  $\chi^2$  was increased by a given factor. This factor was calculated for each set of curves for the degrees of freedom (DOF) given to obtain a probability of 0.68 which corresponds to a  $1\sigma$  uncertainty. The estimated errors are believed to be rather conservative<sup>29</sup> since they are about a factor of three larger than the ones that correspond to  $1\sigma$  uncertainty.

Table 1 lists the rate constants measured for the reaction of *p*-cymene with OH radicals at the indicated temperatures, pressures and concentration range. Given errors for the temperature and pressure represent the standard deviation of those values for the respective set of experiments. Similar to Koch *et al.*,<sup>26</sup> and Bohn and Zetzsch,<sup>29</sup> the rate constants observed at constant temperature and pressure were calculated by fitting sets of  $N$  biexponential decays simultaneously.

#### 3.2 Background reactivity of OH radicals ( $k_2$ )

Reaction (R3) includes the loss of OH radicals by their reactions with impurities that may enter the reactor through tubing connections or ourgassing. This reaction also includes the only minor and approximately exponential diffusion loss of the OH radicals from the photolytic production zone, which is defined by the flash lamp, where the Xe lamp contains a spherical mirror (Technical Manual Perkin Elmer FX 1165). The loss rate constant  $k_2$  at room temperature was found to be  $(22.2 \pm 5.7) \text{ s}^{-1}$  using the N<sub>2</sub> spark lamp and  $(9.8 \pm 4.5) \text{ s}^{-1}$  for the Xe flash lamp, not significantly dependent on total pressure and decreasing slightly with increasing temperature, reaching  $(8.1 \pm 3.6) \text{ s}^{-1}$  at 413 K using the Xe lamp. A weighted regression fit for the function  $k_2 = x_0 \exp(y/T)$  is represented by the line in Fig. 2, with calculated values of  $x_0$  and  $y$  of  $(3 \pm 2) \text{ s}^{-1}$  and  $(430 \pm 250) \text{ K}$ , respectively, and a coefficient of determination,  $R^2$ , of only 10%.

A complete understanding of this parameter is not of great importance, as its small variation does not affect the determination of the other combined constants ( $k_{1a} + k_{1b}$ ,  $k_{1a} k_{-1a}$  and  $k_{-1a} + k_3$ ). It was estimated that if  $k_2$  was kept at a fixed value of  $10 \text{ s}^{-1}$  for the given temperature range, the difference between the new and the old parameters would not exceed about 12% at temperatures below 330 K and above 354 K. Between these

**Table 1** Rate constants  $a_0 = k_2$ ,  $a = k_{1a} + k_{1b}$ ,  $bc = k_{-1a} k_{1a}$  and  $d = k_{-1a} + k_3$  in the reaction system of *p*-cymene with OH radicals at given temperatures

$T/K$	$[p\text{-Cymene}]/10^{12} \text{ cm}^{-3}$	$N^g$	$k_2/s^{-1}$	$(k_{1a} + k_{1b})/10^{-12} \text{ cm}^3 \text{ s}^{-1}$	$(k_{1a} \times k_{-1a})/10^{-12} \text{ cm}^3 \text{ s}^{-2}$	$(k_{-1a} + k_3)/s^{-1}$
$297.2 \pm 0.4^f$	4.9–28.9	19	$22 \pm 6$	$16.4 \pm \begin{smallmatrix} 0.8 \\ 1 \end{smallmatrix}$	$90 \pm 9$	$10.4 \pm 0.1$
$299 \pm 0.2$	5.3–35.4	24	$10 \pm 4$	$14.9 \pm \begin{smallmatrix} 0.8 \\ 0.7 \end{smallmatrix}$	$73 \pm \begin{smallmatrix} 10 \\ 9 \end{smallmatrix}$	$14.5 \pm 0.1$
$309.9 \pm 0.7^f$	5.3–28.5	19	$11 \pm 5$	$15.9 \pm \begin{smallmatrix} 1 \\ 0.9 \end{smallmatrix}$	$234 \pm 20$	$24 \pm 2$
$314.6 \pm 0.5$	5.0–40.4	43	$3 \pm \begin{smallmatrix} 3 \\ 2 \end{smallmatrix}$	$12.1 \pm \begin{smallmatrix} 0.9 \\ 0.8 \end{smallmatrix}$	$204 \pm 30$	$33 \pm 3$
$317 \pm 0.2$	8.9–43.3	12	$17 \pm 6$	$11.7 \pm 0.7$	$221 \pm \begin{smallmatrix} 30 \\ 20 \end{smallmatrix}$	$38 \pm 3$
$317 \pm 0.2^f$	5.2–28.4	19	$16 \pm 4$	$15.8 \pm \begin{smallmatrix} 1 \\ 0.9 \end{smallmatrix}$	$412 \pm 4$	$41 \pm 3$
$322 \pm 1^f$	5.1–28.8	17	$12 \pm 3$	$13 \pm 1$	$401 \pm \begin{smallmatrix} 4 \\ 20 \end{smallmatrix}$	$49 \pm \begin{smallmatrix} 5 \\ 4 \end{smallmatrix}$
$324.2 \pm 0.1$	12.4–44.7	15	$16 \pm \begin{smallmatrix} 9 \\ 7 \end{smallmatrix}$	$10.1 \pm 1$	$259 \pm 40$	$50 \pm \begin{smallmatrix} 5 \\ 4 \end{smallmatrix}$
$326 \pm 2$	6.9–16.9	7	$10 \pm \begin{smallmatrix} 6 \\ 4 \end{smallmatrix}$	$9 \pm 2$	$209 \pm \begin{smallmatrix} 100 \\ 70 \end{smallmatrix}$	$41 \pm \begin{smallmatrix} 10 \\ 8 \end{smallmatrix}$
$325.9 \pm 0.2$	9.3–33.2	32	$13 \pm 5$	$9.4 \pm \begin{smallmatrix} 0.9 \\ 0.8 \end{smallmatrix}$	$228 \pm \begin{smallmatrix} 40 \\ 30 \end{smallmatrix}$	$49 \pm \begin{smallmatrix} 5 \\ 4 \end{smallmatrix}$
$326.5 \pm 0.4^f$	5.0–28.9	12	$17 \pm 4$	$13 \pm \begin{smallmatrix} 2 \\ 1 \end{smallmatrix}$	$549 \pm 5$	$66 \pm \begin{smallmatrix} 8 \\ 7 \end{smallmatrix}$
$327.3 \pm 0.1$	7.7–19.9	9	$11 \pm 5$	$7.97 \pm 1$	$138 \pm \begin{smallmatrix} 50 \\ 40 \end{smallmatrix}$	$39 \pm \begin{smallmatrix} 7 \\ 6 \end{smallmatrix}$
$328.5 \pm 0.1$	7.2–32.6	44	$11 \pm 5$	$8.73 \pm \begin{smallmatrix} 0.7 \\ 0.8 \end{smallmatrix}$	$233 \pm 40$	$55 \pm 5$
$330 \pm 0.2$	7.5–43.5	19	$10 \pm 4$	$8.01 \pm \begin{smallmatrix} 1 \\ 0.9 \end{smallmatrix}$	$191 \pm \begin{smallmatrix} 60 \\ 50 \end{smallmatrix}$	$50 \pm \begin{smallmatrix} 8 \\ 7 \end{smallmatrix}$
$332 \pm 0.2$	7.1–33.3	52	$12 \pm 3$	$6.42 \pm \begin{smallmatrix} 0.7 \\ 0.3 \end{smallmatrix}$	$109 \pm \begin{smallmatrix} 30 \\ 20 \end{smallmatrix}$	$40 \pm 5$
$334.1 \pm 0.4$	4.9–40.8	15	$3 \pm \begin{smallmatrix} 2 \\ 1 \end{smallmatrix}$	$7.3 \pm \begin{smallmatrix} 2 \\ 0.9 \end{smallmatrix}$	$207 \pm \begin{smallmatrix} 100 \\ 90 \end{smallmatrix}$	$60 \pm 20$
$334.3 \pm 0.3$	7.4–33.1	11	$16 \pm 3$	$6.05 \pm 0.06$	$136 \pm \begin{smallmatrix} 50 \\ 30 \end{smallmatrix}$	$50 \pm 7$
$335.4 \pm 0.1$	9.2–27.6	15	$13 \pm 4$	$5.27 \pm \begin{smallmatrix} 0.1 \\ 0.05 \end{smallmatrix}$	$80 \pm \begin{smallmatrix} 30 \\ 20 \end{smallmatrix}$	$38 \pm \begin{smallmatrix} 7 \\ 6 \end{smallmatrix}$
$335.6 \pm 0.3$	6.8–40.2	15	$13 \pm 3$	$4.92 \pm 0.05$	$82 \pm \begin{smallmatrix} 40 \\ 20 \end{smallmatrix}$	$35 \pm \begin{smallmatrix} 7 \\ 6 \end{smallmatrix}$
$336.2 \pm 0.1$	7.3–33.6	59	$12 \pm 2$	$5.28 \pm 0.05$	$76 \pm 20$	$38 \pm 5$
$338.0 \pm 0.2^f$	4.9–28.6	17	$15 \pm 2$	$6.13 \pm \begin{smallmatrix} 1 \\ 0.2 \end{smallmatrix}$	$165 \pm \begin{smallmatrix} 80 \\ 50 \end{smallmatrix}$	$50 \pm 10$
$340 \pm 1$	8.0–42.7	28	$9 \pm 2$	$5.0 \pm 0.1$	$97 \pm \begin{smallmatrix} 40 \\ 30 \end{smallmatrix}$	$48 \pm \begin{smallmatrix} 9 \\ 7 \end{smallmatrix}$
$343.5 \pm 0.2$	7.1–43.0	12	$6 \pm 2$	$4.96 \pm \begin{smallmatrix} 0.2 \\ 0.1 \end{smallmatrix}$	$98 \pm \begin{smallmatrix} 50 \\ 30 \end{smallmatrix}$	$50 \pm 10$
$344.3 \pm 0.4^f$	4.8–34.3	34	$16 \pm 2$	$5.54 \pm \begin{smallmatrix} 0.1 \\ 0.4 \end{smallmatrix}$	$164 \pm \begin{smallmatrix} 70 \\ 50 \end{smallmatrix}$	$70 \pm 10$
$345.2 \pm 0.1$	7.5–38.0	17	$7 \pm 2$	$4.97 \pm \begin{smallmatrix} 0.3 \\ 0.1 \end{smallmatrix}$	$92 \pm \begin{smallmatrix} 30 \\ 40 \end{smallmatrix}$	$50 \pm \begin{smallmatrix} 10 \\ 9 \end{smallmatrix}$
$348 \pm 0.5$	7.6–43.0	14	$9 \pm 2$	$4.44 \pm 0.04$	$70 \pm \begin{smallmatrix} 30 \\ 20 \end{smallmatrix}$	$50 \pm 10$
$348.9 \pm 0.1$	6.8–40.5	37	$3 \pm \begin{smallmatrix} 3 \\ 2 \end{smallmatrix}$	$5.05 \pm 0.05$	$82 \pm \begin{smallmatrix} 70 \\ 40 \end{smallmatrix}$	$60 \pm 20$
$353.5 \pm 0.1$	7.4–37.7	14	$7 \pm 2$	$4.6 \pm 0.1$	$86 \pm \begin{smallmatrix} 60 \\ 30 \end{smallmatrix}$	$70 \pm 20$
$353.8 \pm 0.1$	7.0–27.4	31	$11 \pm 1$	$4.18 \pm 0.04$	$30 \pm \begin{smallmatrix} 7 \\ 5 \end{smallmatrix}$	$36 \pm \begin{smallmatrix} 5 \\ 4 \end{smallmatrix}$
$368.9 \pm 0.1$	7.7–33.1	20	$7 \pm 2$	$4.26 \pm \begin{smallmatrix} 0.09 \\ 0.04 \end{smallmatrix}$	$6 \pm \begin{smallmatrix} 3 \\ 2 \end{smallmatrix}$	$20 \pm \begin{smallmatrix} 7 \\ 1 \end{smallmatrix}$
$382.8 \pm 0.1$	9.0–44.2	12	$9 \pm 2$	$4.05 \pm 0.04$	$4 \pm \begin{smallmatrix} 2 \\ 1 \end{smallmatrix}$	$17.8 \pm 0.2$
$382.8 \pm 0.1$	7.0–27.7	13	$5.2 \pm \begin{smallmatrix} 1 \\ 0.9 \end{smallmatrix}$	$4.22 \pm 0.04$	$2.1 \pm \begin{smallmatrix} 1 \\ 0.6 \end{smallmatrix}$	$11.3 \pm \begin{smallmatrix} 0.1 \\ 0.2 \end{smallmatrix}$
$384.4 \pm 0.1$	7.3–43.6	27	$6 \pm 2$	$4.48 \pm 0.04$	$2.3 \pm \begin{smallmatrix} 2 \\ 0.7 \end{smallmatrix}$	$9.51 \pm 0.1$

Table 1 (continued)

$T/K$	$[p\text{-Cymene}]/10^{12} \text{ cm}^{-3}$	$N^g$	$k_2/s^{-1}$	$(k_{1a} + k_{1b})/10^{-12} \text{ cm}^3 \text{ s}^{-1}$	$(k_{1a} \times k_{-1a})/10^{-12} \text{ cm}^3 \text{ s}^{-2}$	$(k_{-1a} + k_3)/s^{-1}$
$386.9 \pm 0.1$	7.2–43.1	12	$6 \pm 1$	$4.56 \pm \begin{smallmatrix} 0.09 \\ 0.05 \end{smallmatrix}$	$2.2 \pm \begin{smallmatrix} 1 \\ 0.9 \end{smallmatrix}$	$12.4 \pm 0.1$
$403.9 \pm 0.1$	7.1–47.2	12	$10 \pm 2$	$4.8 \pm \begin{smallmatrix} 0.1 \\ 0.05 \end{smallmatrix}$	$2.5 \pm \begin{smallmatrix} 1 \\ 0.9 \end{smallmatrix}$	$9.93 \pm 0.1$
$406 \pm 1^a$	7.6–44.2	9	$9 \pm 2$	$4.95 \pm \begin{smallmatrix} 0.2 \\ 0.2 \end{smallmatrix}$	$3 \pm \begin{smallmatrix} 2 \\ 1 \end{smallmatrix}$	$9.36 \pm 0.09$
$408 \pm 2^e$	9.6–40.3	12	$11 \pm 3$	$4.96 \pm \begin{smallmatrix} 0.1 \\ 0.05 \end{smallmatrix}$	$7 \pm \begin{smallmatrix} 5 \\ 3 \end{smallmatrix}$	$18.8 \pm 0.2$
$407.6 \pm 0.7^d$	11.1–42.0	9	$9 \pm \begin{smallmatrix} 5 \\ 4 \end{smallmatrix}$	$5.12 \pm 0.05$	$8 \pm \begin{smallmatrix} 6 \\ 4 \end{smallmatrix}$	$20 \pm \begin{smallmatrix} 20 \\ 1 \end{smallmatrix}$
$408.3 \pm 0.9^b$	8.8–40.7	12	$12 \pm 3$	$4.85 \pm \begin{smallmatrix} 0.1 \\ 0.05 \end{smallmatrix}$	$4 \pm \begin{smallmatrix} 3 \\ 2 \end{smallmatrix}$	$14.7 \pm 0.1$
$413 \pm 1^c$	10.3–45.0	9	$8 \pm 4$	$5.34 \pm \begin{smallmatrix} 0.05 \\ 0.2 \end{smallmatrix}$	$5 \pm \begin{smallmatrix} 4 \\ 2 \end{smallmatrix}$	$15.4 \pm 0.2$

<sup>a</sup>  $296 \pm 5$  mbar. <sup>b</sup>  $384 \pm 16$  mbar. <sup>c</sup>  $463 \pm 15$  mbar. <sup>d</sup>  $491 \pm 56$  mbar. <sup>e</sup>  $588 \pm 7$  mbar. <sup>f</sup>  $259.4 \pm 0.2$  mbar. <sup>g</sup> Number of measurements.

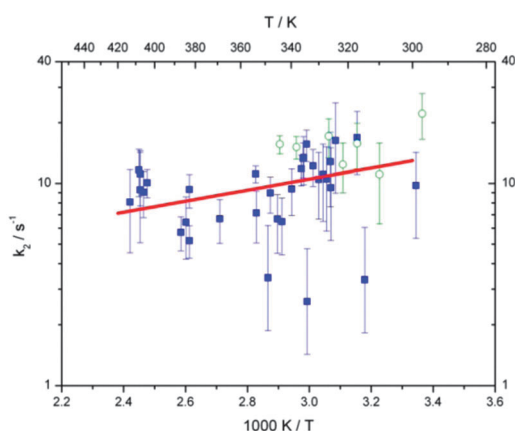


**Fig. 2** The Arrhenius plot for the background loss of OH,  $k_2$ , with the regression line. Solid blue squares were obtained using the Xe flash lamp as the photolytic source while the open green circles were obtained by using the  $N_2$  spark discharge lamp.

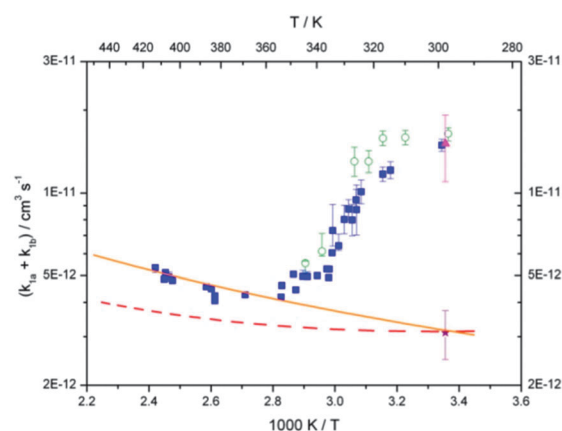


**Fig. 3** The Arrhenius plot of the total rate constant (addition plus abstraction) for the reaction between OH and *p*-cymene. Data obtained using the Xe flash lamp as photolytic source are marked as solid squares (in several cases statistical errors are smaller than the symbols), those obtained by using the  $N_2$  spark discharge lamp as open circles. The asterisk represents the abstraction for *p*-cymene measured by Aschmann *et al.*,<sup>10</sup> at 298 K; the triangle represents the total rate constant from a chamber experiment at 298 K by Corchnoy and Atkinson,<sup>9</sup> the dashed line is the estimated abstraction using Structure Activity Relationships (SARs);<sup>37</sup> the solid line represents an extrapolation of high temperature data down to room temperature (see Section 3.3).

temperatures the model becomes very unstable as will be shown below.

### 3.3 Abstraction and addition channels ( $k_{1a} + k_{1b}$ )

The solution of the differential equation system (eqn (4)–(6)) does not allow us to separate the addition ( $k_{1a}$ ) and abstraction ( $k_{1b}$ ) rate constants, but only to determine the sum of both. The total rate constants determined in this investigation at 297 K using the  $N_2$  spark lamp,  $(16.4 \pm 1.1) \times 10^{-12} \text{ cm}^3 \text{ s}^{-1}$ , and at 299 K using the Xe flash lamp,  $(14.9 \pm 0.8) \times 10^{-12} \text{ cm}^3 \text{ s}^{-1}$ , agree within the calculated errors and they agree well with the value obtained by Corchnoy and Atkinson<sup>9</sup> in a chamber study at 298 K  $(15.1 \pm 4.1) \times 10^{-12} \text{ cm}^3 \text{ s}^{-1}$  (triangle in Fig. 3). On the other hand, the higher value obtained by the  $N_2$  spark lamps is somewhat suspect because of the significantly higher  $a_0$  value, indicating an influence of minor impurities in this first series of runs.

The total rate constants observed in our study decrease slowly at temperatures lower than 320 K and then their decrease becomes steepest at  $T \sim 330$  K and flattens again until around

$T \sim 360$  K. At temperatures higher than 360 K, the total rate constants increase slowly again, mainly due to abstraction. At room temperature, the total rate constant for OH and *p*-cymene is quite similar to the ones measured for *m*-xylene and *p*-xylene. Doyle *et al.*,<sup>38</sup> Hansen *et al.*,<sup>39</sup> Lloyd *et al.*,<sup>40</sup> Perry *et al.*,<sup>13</sup> Ravishankara *et al.*,<sup>41</sup> Cox *et al.*,<sup>42</sup> Nicovich *et al.*,<sup>43</sup> Ohta and Ohyama,<sup>44</sup> Edney *et al.*,<sup>45</sup> and Atkinson and Aschmann<sup>46</sup> reported rate constants to range from 18.8 to  $25.4 \times 10^{-12} \text{ cm}^3 \text{ s}^{-1}$  for *m*-xylene, and between  $10.7$  and  $15.3 \times 10^{-12} \text{ cm}^3 \text{ s}^{-1}$  for *p*-xylene. The rate constant obtained in this work is twice as large as the one found for a substituted benzene with only one isopropyl group, isopropyl benzene, with reported values at room temperature of  $(7.79 \pm 0.50) \times 10^{-12} \text{ cm}^3 \text{ s}^{-1}$  by Ravishankara *et al.*,<sup>41</sup> and  $(6.1 \pm 0.33) \times 10^{-12} \text{ cm}^3 \text{ s}^{-1}$  by Ohta and Ohyama,<sup>44</sup> resulting in an arithmetic mean of  $6.95 \times 10^{-12} \text{ cm}^3 \text{ s}^{-1}$ .

This kinetic result is consistent with the activating property of the additional methyl group in the *para* position according to the Hammett equation.<sup>50</sup>

As suggested by Zetzsch<sup>50</sup> and adopted by Kwok and Atkinson,<sup>37</sup> the Hammett constants for electrophilic addition in aqueous solution obtained by Brown and Okamoto<sup>51</sup> can be used to estimate the rate constant for the addition of OH to *p*-cymene in the gas phase.

Results of the calculation using the EPI (Estimation Program Interface)<sup>47</sup> Suite do not show good agreement with our already published results on *p*-xylene.<sup>48</sup> The measured overall rate constant for these two compounds was found to be twice as high as the ones expected using Hammett constants (see Table 2). Only for the OH + isopropylbenzene reaction the calculation and the measurement are in agreement. It is clear that the structure activity relationship (SAR) only gives a rough estimate and that such SARs are convenient but need to be improved.

This prediction does not yet consider any inductive/mesomeric influence of the isopropyl group on the abstraction channel from the methyl group, but this would be negligible, as follows from the average for abstraction from benzylic methyl groups suggested in the review by Atkinson and Aschmann.<sup>46</sup>

Kwok and Atkinson<sup>37</sup> reported a way of estimating the contribution of the abstraction to the total rate constant, based on the SARs by comparing related compounds. The molecule *p*-cymene has ten aliphatic hydrogen atoms that could be abstracted by an OH radical (see Fig. 4). Hydrogen atoms directly attached to the aromatic ring (a and b in Fig. 4) are not important for the estimation of the abstraction at room temperature, as observed previously for the reaction of OH radicals with benzene where the abstraction rate constant is about  $0.5 \times 10^{-13} \text{ cm}^3 \text{ s}^{-1}$  for the six equivalent H atoms.<sup>13</sup>

**Table 2** Estimated rate constants using Hammett constants for electrophilic addition and measured overall rate constants at  $T = 298 \text{ K}$

Compound	Estimated rate constant ( $\times 10^{-12} \text{ cm}^3 \text{ s}^{-1}$ ) <sup>47</sup>	Measured rate constant ( $\times 10^{-12} \text{ cm}^3 \text{ s}^{-1}$ )
<i>p</i> -Xylene	6.51	14.3 <sup>48,49</sup>
<i>p</i> -Cymene	8.54	15.7 (this work)
Isopropylbenzene	6.90	6.3 <sup>49</sup>

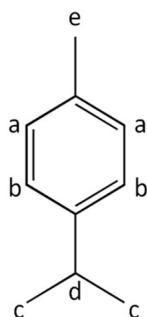


**Fig. 4** The *p*-cymene molecule with indicated non-equivalent C-H bonds.

Rate constants for H-atom abstraction from other groups (atoms c, d and e in Fig. 4) can be estimated as follows:

$$k(\text{CH}_3\text{-X}) = k_{\text{prim}}F(\text{X}) \quad (7)$$

$$k(\text{X-CH(Y)-Z}) = k_{\text{tert}}F(\text{X})F(\text{Y})F(\text{Z}) \quad (8)$$

$$k_{\text{abs}} = 3k(\text{CH}_3\text{-X}) + k(\text{X-CH(Y)-Z}) \quad (9)$$

$$k_{\text{prim}} = 4.49 \times 10^{-18} (T/\text{K})^2 \exp(-320 \text{ K}/T) \quad (10)$$

$$k_{\text{tert}} = 2.12 \times 10^{-18} (T/\text{K})^2 \exp(+696/T) \quad (11)$$

where  $F(\text{X})$ ,  $F(\text{Y})$  and  $F(\text{Z})$  are the substituent factors for the groups X, Y, and Z and  $k_{\text{prim}}$  and  $k_{\text{tert}}$  are the group rate constants for abstraction from  $-\text{CH}_3$  and  $-\text{CH}$  for a standard aliphatic non-aromatic substituent.<sup>37</sup>

In the case of *p*-cymene, there is no information on the substituent factors available other than for  $F(-\text{CH}_3) = 1$ . As a rough simplification it was assumed that the substituent factors for the groups c, d and e presented in Fig. 4 have the same value.

$$F(\text{X})_c = F(\text{X})_e = F(\text{X})_d = F \quad (12)$$

$$k_{\text{abs}} = 3k_{\text{prim}}F + k_{\text{tert}}F \quad (13)$$

Aschmann *et al.*<sup>10</sup> measured the formation yields of 4-methylacetophenone (the major product formed after the H-atom abstraction from the isopropyl group) from the reaction between OH and *p*-cymene in a teflon chamber at  $297 \pm 2 \text{ K}$  and 1 atm pressure of dry pure air. They found that the H-atom abstractions from the methyl and isopropyl group account for  $20 \pm 4\%$  of the total rate constant, which would mean that in this work the rate constant for the abstraction channel at room temperature should be  $(3.1 \pm 0.7) \times 10^{-12} \text{ cm}^3 \text{ s}^{-1}$  (asterisk in Fig. 3). With this value, and calculating  $k_{\text{prim}}$  and  $k_{\text{tert}}$  at 298 K using eqn (10) and (11), the value for  $F$  can be easily found ( $F = 1.33 \pm 0.27$ ). This value is dependent on the temperature in the following way:

$$F = \exp(E_x/T) \quad (14)$$

$E_x$  was found to be 85 K. Using eqn (10), (11) and (13) with an  $E_x$  of 85 K, an estimate of the abstraction can be made for *p*-cymene. This estimation is shown as a red dashed line in Fig. 3, and it can be seen how the increase of the measured data for temperatures higher than 380 K is consistent with the estimated abstraction at these temperatures within the applied approximations.

At high temperatures the reversible addition becomes negligible compared to the irreversible abstraction, and thus high temperature data can be used to estimate the H-atom abstraction. In this work, the obtained total rate constants for temperatures greater than 380 K and the abstraction value at room temperature reported by Aschmann *et al.*<sup>10</sup> were used. A function of the form:  $k = A (T/\text{K})^2 \exp(-E/RT)$  was fitted to the observations at those temperatures, obtaining values for  $A$  of  $2 \times 10^{-17} \text{ cm}^3 \text{ s}^{-1}$  and for  $-E/RT$  of 170 K. This function is shown as a solid line in Fig. 3.

### 3.4 Forward and backward reactions ( $k_{1a}$ $k_{-1a}$ )

The analytical solution to the differential equation system is only able to determine the contributions of the forward and backward reactions as a product of both rate constants. From the Arrhenius plot of this product (Fig. 5) only the combined activation energy can be calculated. Between room temperature and 324 K the product of both rate constants increases with an activation energy of  $45 \text{ kJ mol}^{-1}$ , then it starts to decrease very quickly with an activation energy of  $-78 \text{ kJ mol}^{-1}$  until around 387 K where it starts to increase again with an activation energy of  $+32 \text{ kJ mol}^{-1}$ .

The change in the slope, that is, the change in the sign of the activation energy, may indicate that the system does not fully follow the mechanism proposed in this paper. The second change in the slope could be due to the increasing importance of the abstraction channel at given higher temperatures. On the other hand, the product  $k_{1a} k_{-1a}$  should be unaffected by  $k_{1b}$  if the proposed model is correct.

### 3.5 Unimolecular decay and background loss of the adduct ( $k_{-1a} + k_3$ )

The last parameter that can be directly calculated from the OH radical decay curves includes the sum of the unimolecular decay of the adduct and the rate constant for background loss. As in the case of the OH radicals,  $k_3$  is the rate constant that represents background reactions of the adduct with any impurities that might be present in the cell. The Arrhenius plot for these combined reactions of the adduct is shown in Fig. 6. It is very interesting to note that a similar behaviour is observed as before for the product of forward and backward reaction rate constants, and also at the same temperatures. Weighted fits of the Arrhenius plot between room temperature and 324, 324 and 387 and above 387 K allow us to calculate the activation energy of these three temperature ranges to be 48,  $-27$  and  $75 \text{ kJ mol}^{-1}$ . Again, this change in the slope of the curve at 324 and 387 K indicates that the proposed mechanism could be incomplete and that other reactions are taking place at mid temperatures.

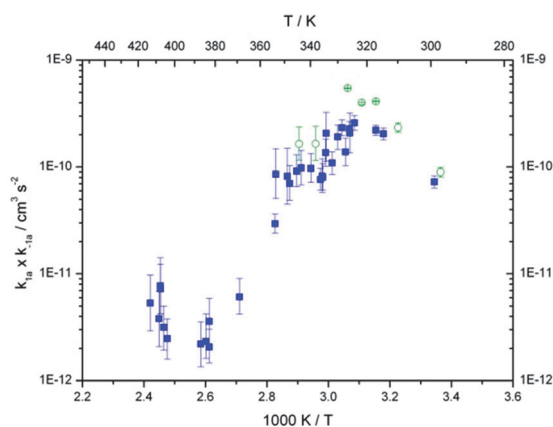


**Fig. 5** The Arrhenius plot of the product of the forward and backward reaction rate constants for *p*-cymene. Data depicted as blue squares were obtained using the Xe flash lamp as the photolytic source while data depicted as green open circles were obtained using the  $\text{N}_2$  spark discharge lamp.

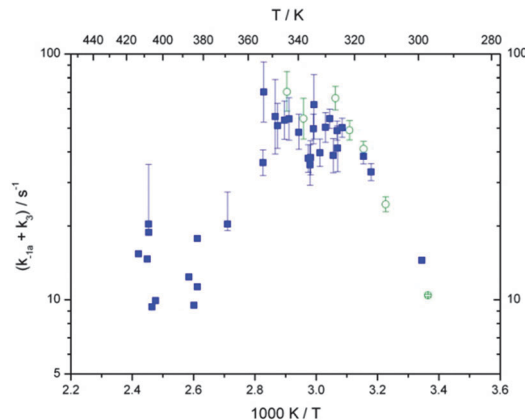


**Fig. 6** Arrhenius plot of the unimolecular decay plus background loss rate constants of the adduct. The blue squares mark data obtained using the Xe flash lamp as the photolytic source while the green open circles mark those obtained using the  $\text{N}_2$  spark discharge lamp.

### 3.6 Equilibrium constant ( $K_{\text{eq}}$ )

The equilibrium rate constant for the reaction between *p*-cymene and the OH radical was determined using the measured rate constants for the individual processes. This can be done by using eqn (15) and calculating the H-atom abstraction as explained above (Section 3.3) to be described by the expression:  $k_{\text{abs}} = 2 \times 10^{-17} (T/\text{K})^2 \exp(+170 \text{ K}/T) \text{ cm}^3 \text{ s}^{-1}$ . The equilibrium constant follows the same behaviour as presented before with two clearly defined temperature ranges. At temperatures higher than 384 K no constants can be calculated due to the approximation used to estimate the abstraction (reversible addition at temperature higher than 384 K is negligible against the abstraction). Plots of the van't Hoff equation are presented in Fig. 7 and lead to  $K_{\text{eq}} = 6 \times 10^{-26} \exp(9700 \text{ K}/T) \text{ cm}^3$  at temperatures below 325 K and  $K_{\text{eq}} = 2 \times 10^{-36} \exp(17000 \text{ K}/T) \text{ cm}^3$  at temperatures above 320 K. The equilibrium constant can be related to the standard reaction enthalpy and entropy using eqn (16),

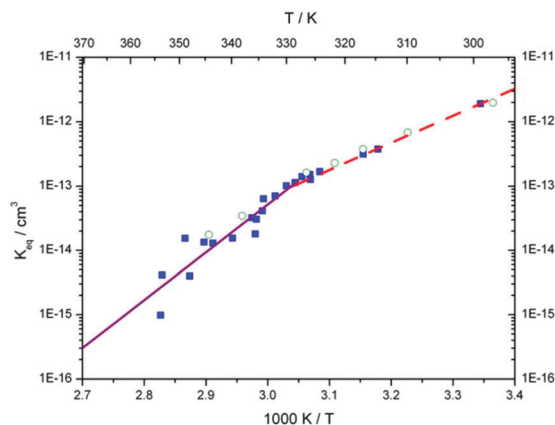


**Fig. 7** Van't Hoff plot of the equilibrium constant. Solid square data were obtained using the Xe flash lamp as the photolytic source while the open green circles data were obtained using the  $\text{N}_2$  spark discharge lamp. The red dashed line is expressed by:  $K_{\text{eq}} = 2 \times 10^{-26} \exp(9700 \text{ K}/T) \text{ cm}^3$ . The blue solid line is expressed by  $K_{\text{eq}} = 2 \times 10^{-36} \exp(17000 \text{ K}/T) \text{ cm}^3$ .

and a standard enthalpy change of  $-74 \text{ kJ mol}^{-1}$  and an entropy of  $-100 \text{ J K}^{-1} \text{ mol}^{-1}$  were found at temperatures below 324 K and a standard enthalpy change of  $-324 \text{ kJ mol}^{-1}$  and an entropy change of  $-147 \text{ J K}^{-1} \text{ mol}^{-1}$  at temperatures above 324 K.

$$K_{\text{eq}} = \frac{k_{1a}}{k_{-1a}} = \frac{((k_{1a} + k_{1b}) - k_{\text{abs}})^2}{k_{1a}k_{-1a}} \quad (15)$$

$$K_{\text{eq}} = \frac{k_b T}{P^{\theta}} \exp\left(\frac{-\Delta H}{RT} + \frac{\Delta S}{R}\right) \quad (16)$$

### 3.7 Goodness of the biexponential fit

Reduced  $\chi^2$  values, *i.e.*,  $\chi^2$  divided by the degrees of freedom, DOF, were calculated for each measurement and are presented in Fig. 8. It can be observed that between  $T = 317$  and  $344 \text{ K}$  the values for the reduced  $\chi^2$  are very high, indicating that the model used does not explain our observations. These results indicate that the current model cannot explain processes occurring at temperatures where the addition reaction channel appears to be more important than the abstraction channel. It is also evident that the addition path changes somehow with increasing temperature, indicating a possible OH-*p*-cymene adduct formation with a different energy or an isomerization into more stable adducts.

A deeper examination of each decay curve of experiments performed between  $T = 317$  and  $344 \text{ K}$  revealed the presence of a third exponential component that may be indicative of another reversible process taking place. Each curve was fitted to a triexponential model of the form:

$$[\text{OH}](t) = I_1 \exp\left(-\frac{t}{\tau_1}\right) + I_2 \exp\left(-\frac{t}{\tau_2}\right) + I_3 \exp\left(-\frac{t}{\tau_3}\right) \quad (17)$$

The slow component,  $\tau_3^{-1}$ , was found to depend on the temperature and the concentration of *p*-cymene, indicating that this new parameter is not a mathematical artefact but has a chemical origin. The dependence on the temperature is shown in Fig. 9, and it can be seen how  $\tau_3^{-1}$  increases with increasing temperature up to about  $355 \text{ K}$ , where it starts decreasing again.

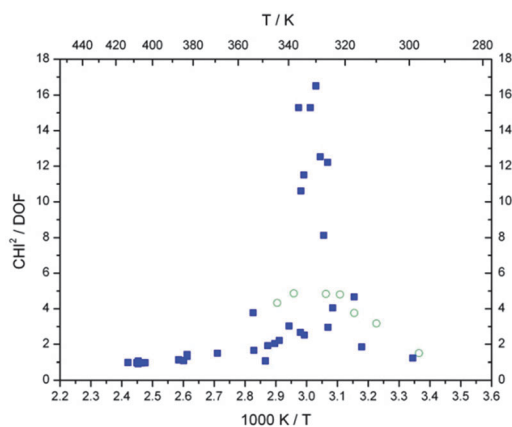


**Fig. 8** Reduced  $\chi^2$  for all the measurements of Table 1. The filled blue squares data were obtained using the Xe flash lamp as the photolytic source and the open green circles data were obtained using the  $\text{N}_2$  spark discharge lamp.

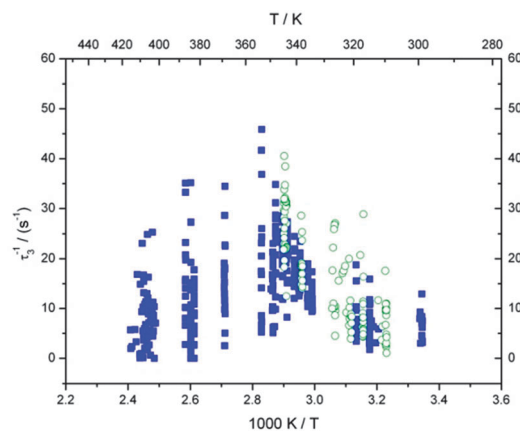


**Fig. 9** The slow component,  $\tau_3^{-1}$ , of the triexponential fit of all measurements. Solid squares were obtained using the Xe flash lamp as the photolytic source while open circles were obtained using the  $\text{N}_2$  spark discharge lamp.

A similar behaviour was observed for the  $\chi^2/\text{DOF}$  (Fig. 8), indicating that the deviations of the proposed biexponential model from our measurements are due to another process between OH and *p*-cymene over the temperature range studied.

The aromatic molecule *p*-cymene differs from the other already studied substituted aromatics (toluene, xylene, mesitylene, hexamethylbenzene) in its symmetry. While these aromatics contain methyl groups as substituents, *p*-cymene contains a methyl and an isopropyl group. The formation of two ipso adducts with different energies can be expected, at two equivalent positions *ortho* to the methyl group, and two other equivalent ones *ortho* to the isopropyl group, making a total of 4 distinguishable adducts. The triexponential behaviour of the OH decay curves implies that an improved evaluation of the observed decays is feasible<sup>29</sup> in order to obtain information about the formation of other adducts. This will be demonstrated in part 2 of this study.

## 4. Conclusions

A simplified model that includes the formation of either one or several undistinguishable adducts was fitted to the observed OH decay curves in the presence of *p*-cymene. The fit procedure was done by simultaneously fitting the model to a set of decay curves at the same temperature and pressure but different *p*-cymene concentrations. Rate constants and Arrhenius expressions were determined and compared with available kinetic data of similar aromatic compounds. The observed slope changes for the determined rate constants around  $324 \text{ K}$  and again around  $387 \text{ K}$  indicated that the chosen model does not perfectly fit our data over the given temperature range, as confirmed by the  $\chi^2/\text{DOF}$  values. Between these temperatures, the OH decay curves were found to be no longer biexponential but triexponential, indicating the formation of more than one single adduct.

## Acknowledgements

This work was supported by the Deutsche Forschungsgemeinschaft (DFG ZE792/6-1) within the French-German CNRS-INSU/DFG

bilateral program ATMOCHEM. We thank Birger Bohn, Forschungszentrum Jülich, for providing IDL routines, and Roger Atkinson, University of California at Riverside, for providing information about the abstraction channels.

## References

- 1 A. Guenther, C. N. Hewitt, D. Erickson, R. Fall, C. Geron, T. Graedel, P. Harley, L. Klinger, M. Lerdau, W. A. McKay, T. Pierce, B. Scholes, R. Steinbrecher, R. Tallamraju, J. Taylor and P. Zimmerman, *J. Geophys. Res.*, 1995, **100**, 8873–8892.
- 2 B. Lamb, D. Gay, H. Westberg and T. Pierce, *Atmos. Environ., Part A*, 1993, **27**, 1673–1690.
- 3 D. C. Degenhardt and D. E. Lincoln, *J. Chem. Ecol.*, 2006, **32**, 725–743.
- 4 S. D. Maleknia, T. M. Vail, R. B. Cody, D. O. Sparkman, T. L. Bell and M. A. Adams, *Rapid Commun. Mass Spectrom.*, 2009, **23**, 2241–2246.
- 5 M. Staudt and L. Lhoutellier, *Tree Physiol.*, 2007, **27**, 1433–1440.
- 6 C. Geron, R. Rasmussen, R. R. Arnsts and A. Guenther, *Atmos. Environ.*, 2000, **34**, 1761–1781.
- 7 A. Gratien, S. N. Johnson, M. J. Ezell, M. L. Dawson, R. Bennett and B. J. Finlayson-Pitts, *Environ. Sci. Technol.*, 2011, **45**, 2755–2760.
- 8 S. M. Aschmann, J. Arey and R. Atkinson, *Atmos. Environ.*, 2011, **45**, 4408–4411.
- 9 S. B. Corchnoy and R. Atkinson, *Environ. Sci. Technol.*, 1990, **24**, 1497–1502.
- 10 S. M. Aschmann, J. Arey and R. Atkinson, *Atmos. Environ.*, 2010, **44**, 3970–3975.
- 11 F. Stuhl and H. Niki, *J. Chem. Phys.*, 1972, **57**, 3677.
- 12 D. D. Davis, W. Bollinger and S. Fischer, *J. Phys. Chem.*, 1975, **79**, 293–294.
- 13 R. A. Perry, R. Atkinson and J. N. Pitts, *J. Phys. Chem.*, 1977, **81**, 296–304.
- 14 F. P. Tully, A. R. Ravishankara, R. L. Thompson, J. M. Nicovich, R. C. Shah, N. M. Kreutter and P. H. Wine, *J. Phys. Chem.*, 1981, **85**, 2262–2269.
- 15 K. Lorenz and R. Zellner, *Ber. Bunsenges. Phys. Chem.*, 1983, **87**, 629–636.
- 16 S. Madronich and W. Felder, *J. Phys. Chem.*, 1985, **89**, 3556–3561.
- 17 T. J. Wallington and M. J. Kurylo, *J. Phys. Chem.*, 1987, **91**, 5050–5054.
- 18 A. Wahner and C. Zetzsch, *J. Phys. Chem.*, 1983, **87**, 4945–4951.
- 19 F. Witte, A. Wahner and C. Zetzsch, *Bull. Soc. Chim. Belg.*, 1983, **92**, 625–626.
- 20 M. Rinke and C. Zetzsch, *Ber. Bunsenges. Phys. Chem.*, 1984, **88**, 55–62.
- 21 F. Witte, E. Urbanik and C. Zetzsch, *J. Phys. Chem.*, 1986, **90**, 3251–3259.
- 22 R. Knispel, R. Koch, M. Siese and C. Zetzsch, *Ber. Bunsenges. Phys. Chem. Chem. Phys.*, 1990, **94**, 1375–1379.
- 23 M. Siese and C. Zetzsch, *Z. Phys. Chemie-Int. J. Res. Phys. Chem. Chem. Phys.*, 1995, **188**, 75–89.
- 24 R. Koch, H. U. Krüger, M. Elend, W. U. Palm and C. Zetzsch, *Int. J. Chem. Kinet.*, 1996, **28**, 807–815.
- 25 R. Koch, W. U. Palm and C. Zetzsch, *Int. J. Chem. Kinet.*, 1997, **29**, 81–87.
- 26 R. Koch, R. Knispel, M. Elend, M. Siese and C. Zetzsch, *Atmos. Chem. Phys.*, 2007, **7**, 2057–2071.
- 27 S. Zhang, R. Strekowski, L. Bosland, A. Monod and C. Zetzsch, *Phys. Chem. Chem. Phys.*, 2011, **13**, 11671–11677.
- 28 S. Zhang, R. S. Strekowski, L. Bosland, A. Monod and C. Zetzsch, *Int. J. Chem. Kinet.*, 2011, **43**, 547–556.
- 29 B. Bohn and C. Zetzsch, *Phys. Chem. Chem. Phys.*, 2012, **14**, 13933–13948.
- 30 S. Zhang, R. S. Strekowski, A. Monod, L. Bosland and C. Zetzsch, *J. Phys. Chem. A*, 2012, **116**, 9497–9506.
- 31 O. C. Bridgeman and E. W. Aldrich, *J. Heat Transfer*, 1964, **86**, 279–286.
- 32 E. G. Linder, *J. Phys. Chem.*, 1931, **35**, 531–535.
- 33 K. A. Kobe, T. S. Okabe, M. T. Ramstad and P. M. Huenner, *J. Am. Chem. Soc.*, 1941, **63**, 3251–3252.
- 34 R. A. McDonald, S. A. Shrader and D. R. Stull, *J. Chem. Eng. Data*, 1959, **4**, 311–313.
- 35 W. Strubell, *J. Prakt. Chem.*, 1964, **26**, 319–323.
- 36 V. Ruzicka Jr, M. Zabransky, K. Ruzicka and V. Majer, *Thermochim. Acta*, 1994, **245**, 121–144.
- 37 E. S. C. Kwok and R. Atkinson, *Atmos. Environ.*, 1995, **29**, 1685–1695.
- 38 G. J. Doyle, A. C. Lloyd, K. R. Darnall, A. M. Winer and J. N. Pitts, *Environ. Sci. Technol.*, 1975, **9**, 237–241.
- 39 D. A. Hansen, R. Atkinson and J. N. Pitts, *J. Phys. Chem.*, 1975, **79**, 1763–1766.
- 40 A. C. Lloyd, K. R. Darnall, A. M. Winer and J. N. Pitts, *J. Phys. Chem.*, 1976, **80**, 789–794.
- 41 A. R. Ravishankara, S. Wagner, S. Fischer, G. Smith, R. Schiff, R. T. Watson, G. Tesi and D. D. Davis, *Int. J. Chem. Kinet.*, 1978, **10**, 783–804.
- 42 R. A. Cox, R. G. Derwent and M. R. Williams, *Environ. Sci. Technol.*, 1980, **14**, 57–61.
- 43 J. M. Nicovich, R. L. Thompson and A. R. Ravishankara, *J. Phys. Chem.*, 1981, **85**, 2913–2916.
- 44 T. Ohta and T. Ohyama, *Bull. Chem. Soc. Jpn.*, 1985, **58**, 3029–3030.
- 45 E. O. Edney, T. E. Kleindienst and E. W. Corse, *Int. J. Chem. Kinet.*, 1986, **18**, 1355–1371.
- 46 R. Atkinson and S. M. Aschmann, *Int. J. Chem. Kinet.*, 1989, **21**, 355–365.
- 47 U. S. EPA, *Estimation Programs Interface Suite TM for Microsoft(r) Windows*, United States Environmental Protection Agency, Washington, DC, USA, 2012.
- 48 R. Atkinson, *J. Phys. Chem. Ref. Data Monogr.*, 1989, 228.
- 49 J. G. Calvert, R. Atkinson, K. H. Becker, R. M. Kamens, J. H. Seinfeld, T. J. Wallington and G. Yarwood, *The Mechanisms of Atmospheric Oxidation of Aromatic Hydrocarbons*, Oxford University Press, Oxford, New York, 2002.
- 50 C. Zetzsch, *Predicting the rate constant of OH addition to aromatics using  $\sigma^+$ -electrophilic substituent constants for mono- and polysubstituted benzenes*, Abstract A11, XVth Informal Conf. on Photochemistry, Stanford, CA, USA, 1982.
- 51 H. C. Brown and Y. Okamoto, *J. Am. Chem. Soc.*, 1958, **80**, 4979–4987.